2013

A facile, low-cost route for the preparation of calcined porous calcite and dolomite and their application as heterogeneous catalysts in biodiesel production

Rui Wang
Guiyang College, wangrui961@gmail.com

Hu Li
Guizhou University

Fei Chang
Guizhou University

Jiafeng Luo
Guizhou University

Milford A. Hanna
University of Nebraska-Lincoln, mhanna1@unl.edu

See next page for additional authors

Catalysis
Science & Technology

RSC Publishing

PAPER

View Article Online
View Journal | View Issue

A facile, low-cost route for the preparation of calcined porous calcite and dolomite and their application as heterogeneous catalysts in biodiesel production†

Cite this: *Catal. Sci. Technol.*, 2013, **3**, 2244

Rui Wang,[ab] Hu Li,[a] Fei Chang,[a] Jiafeng Luo,[a] Milford A. Hanna,[c] Daoyang Tan,[a] Deyu Hu,[a] Yuping Zhang,[a] Baoan Song[a] and Song Yang*[a]

Received 22nd February 2013,
Accepted 3rd May 2013

DOI: 10.1039/c3cy00129f

www.rsc.org/catalysis

Despite their potential for biodiesel synthesis, directly calcined minerals rich in magnesium/calcium carbonates are used at the expense of large amounts of the catalyst, high alcohol loading, long processing times, and severe conditions. We report a facile and low-cost route for preparing calcined porous calcite (CPC) and dolomite (CPD) *via* simple thermal decomposition of the reaction mixtures of natural calcite and dolomite with stearic acid. CPC and CPD, both of which have porous structures, were compared with previously reported catalysts and examined as promising heterogeneous base catalysts under mild conditions. A 40% increase in conversion through CPC and CDC was achieved compared with that achieved through directly calcined minerals. A systematic understanding of the enhancement and deactivation relationships of the products was established by catalyst characterization, including XRD, BET, CO_2-TPD, SEM, TEM, and XPS. The obtained CPC and CPD showed large pore sizes and high active site densities and provided an advantageous environment for transesterification of triglyceride with methanol. CPC and CPD are re-usable and show no loss of activity after regeneration.

Introduction

Biodiesels (fatty acid methyl ester, FAME) have been proposed and accepted as promising environment-friendly alternatives to fossil fuel. Considerable efforts have been devoted toward the exploration and development of ideal feedstocks, highly effective heterogeneous catalysts, and efficient conversion processes.[1,2]

The use of natural magnesium/calcium carbonate-rich minerals as the feedstocks has recently become an interesting approach toward developing low-cost and widely available heterogeneous catalysts for biodiesel production. Such minerals include dolomite, calcite, and waste shells, among others. However, to our disappointment, a satisfactory conversion for transesterification is only achieved in the presence of directly calcined minerals, such as common CaO and MgO, at the expense of large amounts of catalysts (5 wt% to 25 wt%), high molar ratios of methanol to oil (up to 50 : 1), long reaction times (1 h to 5 h), or severe conditions, resulting in high production costs and limited practical applications.[3–6] Recent studies have attributed the poor catalytic performances of common CaO and MgO to their low active site density (ASD) and low special surface area (SSA).[7–10]

To promote the catalytic activities of CaO and MgO, various modified methods have been employed and investigated, such as supercritical drying, calcination in a vacuum or inert gas, nanotechnology, preparation from different precursors, hydration–dehydration, and loading onto supports.[9–13] Nanocrystalline CaO (crystal size = 20 nm; SSA = 90 $m^2\ g^{-1}$) has been developed for biodiesel production, resulting in activity 45 times higher than that of laboratory grade CaO (crystal size = 43 nm; SSA = 1 $m^2\ g^{-1}$).[11] In a study by Kouzu *et al.*,[14] CaO–helium with high ASD (0.12 mmol g^{-1} *vs.* 0.03 mmol g^{-1}) and basic strength ($15.0 < H_- < 18.4$ *vs.* $9.3 < H_- < 15.0$) provided higher conversion compared with that provided by CaO–air (93% *vs.* 10%). Hierarchical macroporous–mesoporous silica sulfonic acid catalysts have been developed, and these show higher activities than HO_3S-SBA-15.[15] All of the enhanced effects observed can be

[a] *State-Local Joint Laboratory for Comprehensive Utilization of Biomass, State Key Laboratory Breeding Base of Green Pesticide and Agricultural Bioengineering, Center for Research and Development of Fine Chemicals, Guizhou University, Guiyang 550025, P.R. China. E-mail: jhzx.msm@gmail.com; Fax: +86 851-829-2170*

[b] *Food and Pharmaceutical Engineering Institute, Guiyang College, Guiyang 550003, P.R. China. E-mail: wangrui961@gmail.com; Fax: +86 851-540-7613*

[c] *Industrial Agricultural Products Center, University of Nebraska, Lincoln, NE 68583-0730, USA. E-mail: mhanna@unlnotes.unl.edu; Fax: +1 402-472-6338*

† Electronic supplementary information (ESI) available: TGA curves of catalyst precursors; characterization for partial catalyst samples. See DOI: 10.1039/c3cy00129f

interpreted in terms of the textural properties of the catalyst. The catalytic performances of CaO and MgO may be logically improved to feature increased active site strengths, ASD, and SSA.

In view of the correlation between physicochemical properties and catalytic activity, an effective route for enhancing the efficiency of methanol adsorption on MgO or CaO surfaces may include the exposure of more active sites and easier reactants accessibility. Porous materials have extensive chemical industrial applications, such as catalysis, separation, and adsorption. However, most porous supports (*e.g.*, SBA-15, MCM-41, Al_2O_3, *etc.*) are poorly or not completely catalytically active for transesterification reactions under mild conditions. Hence, we believe that porous MgO and CaO catalysts with high SSAs, facile mass transportation, and recyclability are highly desirable for heterogeneous biodiesel catalysis. Mesoporous CaO and MgO with high SSAs (257 m^2 g^{-1} and 205 m^2 g^{-1}, respectively) have been reported to exhibit excellent CO_2 adsorption behavior.[16,17] However, the template approach is rather time consuming ($\geq$72 h), expensive, and can limit commercial applications in biodiesel. Takenaka *et al.*[18] reported a facile approach for preparing mesoporous MgO and Ni–MgO using low-cost stearic acid as a catalyst for the hydrogenation of 4-heptanone to 4-heptanol. In the present work, we attempt to synthesize calcined porous calcite (CPC) and calcined porous dolomite (CPD) by thermal decomposition of the reaction mixtures of magnesium, calcium, and stearic acid through a simple strategy based on the study by Takenaka *et al.* The catalytic performances of the obtained catalysts were evaluated in the transesterification of refined *Jatropha curcas* L. oil (JCO), *Euphorbia lathyris* L. oil (ELO), and dewaxing *Sapium sebiferum* L. kernel oil (DSSKO). The correlation between the catalytic performance and physicochemical properties of the modified materials was studied by several characterization techniques, including Brunauer–Emmett–Teller (BET), X-ray diffraction (XRD), temperature-programmed desorption of CO_2 (CO_2-TPD), scanning electron microscopy (SEM), transmission electron microscopy (TEM), and X-ray photoelectron spectroscopy (XPS). The catalytic behavior, reusability, and regeneration of the modified materials were also investigated.

Experimental

Materials

Natural calcite and dolomite powders (400 mesh) were collected from Guizhou Province, China. The elemental compositions of the powders were analyzed using an Oxford INCA-350 energy dispersive X-ray spectrometer, and the components (wt%) were found to be as follows: calcite: Ca 46.2 wt%, Mg 1.2 wt%, C 18.2 wt%, O 33.4 wt%, Si 0.6 wt%, Fe 0.1 wt%, S 0.2 wt%; dolomite: Ca 26.9 wt%, Mg 13.9 wt%, C 10.7 wt%, O 48.1 wt%, Si 0.3 wt%. Analytical reagent-grade stearic acid, methanol, and other agents were purchased from Kermel Chemical Reagent Co., Ltd., Tianjing, China. JCO and ELO were obtained by squeezing JC and EL seeds obtained from Luodian County, Guizhou Province, and Bozhou City, Anhui Province, China. DSSKO was prepared from SS oil purchased from Suizhou Tianfeng Local Product Co., Ltd. (Suizhou, China), according to the method reported in our previous work.[19] These three crude oils were further purified by de-acidification and drying. The acid values of the resulting refined JCO, ELO, and DSSKO were 0.46, 0.27, and 0.19 mg KOH g^{-1}, respectively. The average molecular weights and fatty acid compositions of the oils were determined in our previous work.[19]

Catalyst preparation and regeneration

In a typical synthesis, 60 g of stearic acid was melted at 80 °C. To this melt, 10 g of calcite or dolomite was added with vigorous stirring. The mixture was heated at 100 °C for 1 h and then at 170 °C for 1 h to yield the reaction mixtures of calcium, magnesium, and stearic acid, respectively. CPC and CPD were then prepared through a two-step thermal decomposition program in a tube furnace. The calcination temperatures were determined based on the thermogravimetric analysis (TGA) results shown in Fig. S1.† Both reaction mixtures of calcite–stearic acid and dolomite–stearic acid were heated to 750 °C for 1 h under 50 L h^{-1} air flow, and then continuously calcined at 850 °C, for 1 h in static air. The entire process was performed at a rate of 4 °C min^{-1}. The excess stearic acid was recovered using an air condenser installed at the outlet of the tube furnace. The calcined calcite (CC) and dolomite (CD) were prepared by calcination at 850 °C, respectively, for 1 h in static air at a rate of 4 °C min^{-1}. For comparison, 15 wt% CaO–SBA-15 and mesoporous CaO (MC) were prepared according to the literature.[13,16]

After every transesterification reaction, regenerated CPC (RCPC) and CPD (RCPD) were obtained by washing with *n*-hexane and drying under a vacuum. Recalcination (850 °C for 1 h at 4 °C min^{-1}) was necessary because CaO is susceptible to CO_2 and H_2O poisoning within a few minutes. All catalyst samples were sealed in sample bottles and then stored in a vacuum desiccator containing silica gel and KOH pellets.

Catalyst characterization

The TGA data were collected using a Netzsch STA449C Jupiter TGA/DSC at a heating rate of 4 °C min^{-1} and under pure nitrogen. The morphologies of the catalyst samples were examined by SEM on a Hitachi S-3400 N. The microscopic features were obtained by TEM on a JEOL-2100 system operated at 200 kV. Sample powders were dispersed in anhydrous ethanol by ultrasonication at concentrations of 5 wt% solids. Then, a porous carbon copper grid was dipped into the suspension and then dried under a vacuum at 80 °C for 8 h prior to analysis. N_2 adsorption–desorption isotherms were measured by a Micromeritics TriStar II 3020 system (adsorption of N_2 at 77 K). All samples were degassed for 3 h at 300 °C, before BET analysis. SSA was calculated by the BET method over the relative pressure range P/P_0 = 0.05 to 0.20. The pore size distribution was established from desorption data using the Barrett–Joyner–Halenda (BJH) method. Pore volumes were calculated at a relative pressure of about 0.99. Powder XRD investigation was performed using a Bruker D8 Advanced X-ray diffractometer with Cu Kα radiation (λ = 0.154 nm) at 40 kV and 30 mA with a step size of 0.02. The mean primary crystallite size of the catalysts was determined using the Scherrer equation

from the FWHM of the strongest XRD diffraction peak. ASD results of catalysts were obtained by CO_2-TPD experiments, which were performed using a Xianquan 50 TP-5085 instrument referring to the method proposed by Alonso *et al.*,[8] a 175 mg sample was treated in Ar flow (40 mL min^{-1}) at 1073 K (ramp of 10 K min^{-1}) for 1 h firstly, then 23 vol% CO_2/Ar (20 mL min^{-1}) was used as adsorption gas for 1 min when samples were then cooled down to room temperature, then desorption procedure was preformed from 308 to 1150 K (4 K min^{-1}). The base strength was tested by Hammett indicators.[5] X-ray photoelectron spectroscopy (XPS) was recorded at room temperature using a Kratos Axis Ultra DLD system and a monochromatic Al Kα source operated at 15 keV and 150 W. The detection area was 1200 μm × 800 μm. Charge neutralization was required for all samples and thus accordingly performed. Charge correction was made with the C1s signal of adventitious carbon (C–C or C–H bonds) at 284.8 eV. The residual pressure in the spectrometer chamber was 5×10^{-9} mbar during data acquisition. The calcium and magnesium leached in the biodiesel samples were determined using inductively coupled plasma-atomic emission spectroscopy (Optima 2000DV, PerkinElmer). Pre-treatment of biodiesel samples was performed using the method of Verziu *et al.*[9]

Transesterification catalysis

Catalytic transesterification reactions were performed in a 100 mL three-necked glass flask in an oil bath. The flask was charged with 50.00 g of JCO and the prescribed amounts of methanol and catalyst and then subjected to magnetic mixing. The mixture was vigorously stirred (600 r min^{-1}) for the required reaction time at 338 K in an inert atmosphere (N_2). After the prescribed time, the system was quickly immersed into an ice-salt bath to stop the reaction. The mixture was filtered, and the excess methanol was recovered by rotary evaporation. Then, the liquid phase was transferred into a separatory funnel, allowed to settle overnight, and further separated by centrifugation. The FAME content of the samples were determined by gas chromatography (Agilent 6890GC) equipped with a flame ionization detector. The following chromatographic conditions were applied: inlet temperature = 523 K; detector temperature = 553 K; split ratio = 20 : 1; oven temperature program = 463 K for 3 min, ramp rate = 15 K min^{-1}, up to 513 K, held for 17 min; injection volume = 1 μL; carrier gas = helium, flow rate = 1.0 mL min^{-1}; air flow = 450 mL min^{-1}; and H_2 flow = 40 mL min^{-1}. A GC method based on external standards was adopted to analyze the FAME (wt%) of the biodiesels. The FAME yield was calculated, according to the following equation:

$$\text{FAME yield}(\%) = \frac{\text{Total weight of FAME}}{\text{Total weight of oil}} \times 100\%$$

Results and discussion

Catalyst characterization

Fig. S1† shows the weight loss curves of the catalyst precursors. Natural calcite and dolomite showed major weight losses of 44.64 wt% and 46.93 wt% at 826 °C and 803 °C, respectively. Compared with the TGA curves of the two natural minerals, the weight curves of magnesium stearate and calcium stearate in Fig. S1† revealed that the organic–inorganic precursors were synthesized, but not all of the magnesium/calcium carbonates contained in the two natural minerals are completely converted into magnesium stearate or calcium stearate. Therefore, the obtained products were claimed as reaction mixtures. Fig. S1† indicates that the three reaction mixtures had more weight-loss stages. For example, the thermal decomposition of the calcite–stearic acid melted product (Fig. S1(c)†) can be divided into three major stages. The first stage was from 200 °C to 300 °C, with a weight loss of 14.79 wt%. The second stage was from 300 °C to 560 °C, with a weight loss of 60.27 wt%. The final stage was from 560 °C to 750 °C, with a weight loss of 11.25 wt%. The reaction mixtures of calcite–stearic acid and dolomite–stearic acid showed weight losses of 86.31 wt% and 88.35 wt%, respectively. On the basis of these results, all the precursors were activated by calcination at the major weight loss temperatures.

The morphologies and structures of the as-synthesized catalyst samples were characterized from the XRD patterns (Fig. 1), SEM images (Fig. 2 and Fig. S2†), TEM images (Fig. 3), and N_2 adsorption–desorption isotherms (Fig. 4 and 5). Based on the XRD results (Fig. 1) and previous studies,[10,20] CaO and MgO were confirmed as the major active species on the surface of the catalyst samples. Fig. 1(A) shows that the wide-angle XRD peaks of all the modified materials are broader than those of CC, although all of the catalyst samples are composed of CaO species. This finding indicates the formation of smaller particles and poor crystallites. As an example, the peaks of the CPC sample attributed to crystalline CaO (32.20°, 37.35°, 53.86°, 64.16°, and 67.39°) and $Ca(OH)_2$ (17.99° and 28.80°) were also observed. The mean primary crystallite sizes of the samples were calculated using the Scherrer equation and are listed in Table 1. The primary mean crystal size of calcined calcite (CC, 58 nm) derived from calcite was larger than those of calcined calcium stearate (CCS, 35 nm) and CPC (40 nm). Similar trends were also observed in calcined dolomite (CD), CPD, and calcined magnesium stearate (CMS, Fig. 1(B)), probably because of the formation of identical species from different precursors.[8,21] In Fig. 1(A), all of the samples except CaO–SBA-15 exhibit major Bragg diffraction peaks of CaO after calcination. Although this result is different from that reported by Samart *et al.*,[13] it indicates that the supported CaO is well dispersed in the pores of SBA-15.[22] Moreover, only CaO–SBA-15 featured an ordered mesoporous structure, as evidenced by intense diffraction peaks (inset of Fig. 1(A)) in the low-angle XRD pattern obtained.

SEM images of the as-synthesized catalyst samples are shown in Fig. 2 and Fig. S2†. CC and CD clearly showed massive irregular shapes of agglomerates with large void volumes; the surface of CD was rough and pitted. As a result, CD had a higher SSA (14.3 m^2 g^{-1}, Table 1) than CC (4.1 m^2 g^{-1}, Table 1). When the reaction mixtures of calcite–stearic acid and dolomite–stearic acid were decomposed and converted into CO_2, CaO, and MgO during the calcination, smaller particles were obtained because a large amount of CO_2 escapes from the system.

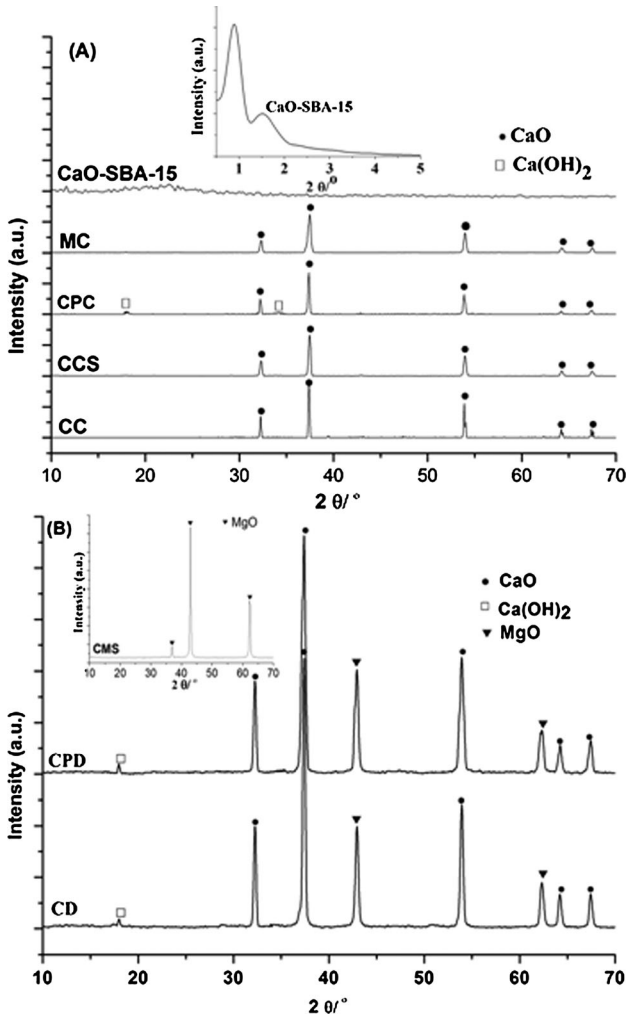

Fig. 1 (A) Wide-angle XRD patterns of catalyst samples: calcined calcite (CC), calcined calcium stearate (CCS), calcined porous calcite (CPC), mesoporous CaO (MC), and CaO–SBA-15; low-angle XRD of CaO–SBA-15 (inset). (B) XRD patterns of catalyst samples: calcined dolomite (CD), calcined porous dolomite (CPD), and calcined magnesium stearate (CMS, inset).

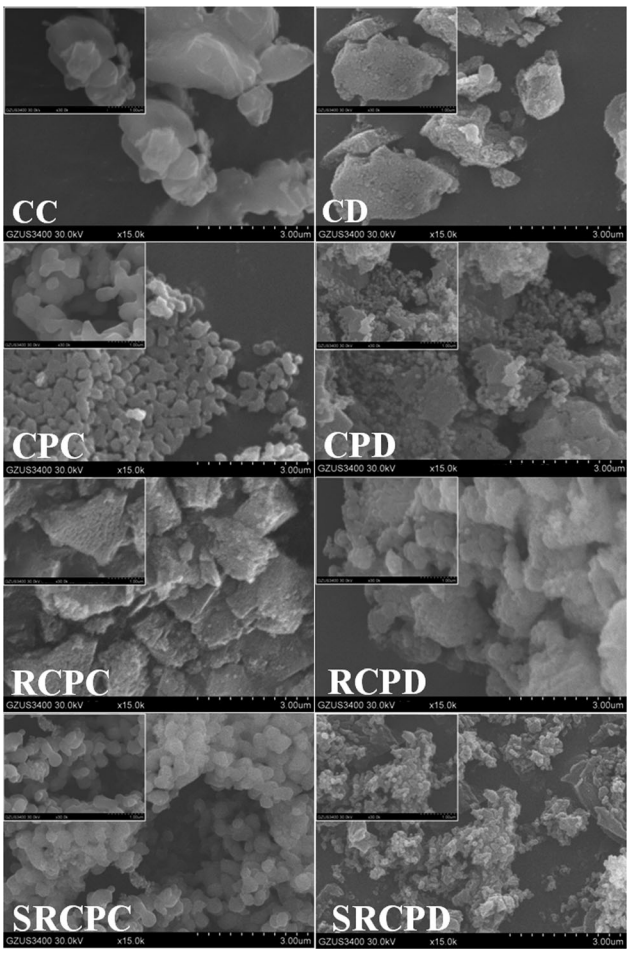

Fig. 2 SEM images of as-synthesized catalyst samples: calcined calcite (CC), calcined dolomite (CD), calcined porous calcite (CPC), calcined porous dolomite (CPD), calcined calcium stearate (CCS), regenerated calcined porous calcite (RCPC), regenerated calcined porous dolomite (RCPD), stearic acid-regenerated CPC (SRCPC), and stearic acid-regenerated CPD (SRCPD).

This phenomenon supports the XRD results (Fig. 1). Consequently, considerable numbers of visible voids were generated in CPC and CPD because of the aggregation and connection of many smaller particles. The N_2 adsorption–desorption isotherms (Fig. 4 and 5) indicate the formation of porous materials that result in high SSAs. CPC exhibited a higher SSA than CC (8.7 $m^2\ g^{-1}$ *vs.* 4.1 $m^2\ g^{-1}$), as summarized in Table 1. Although CCS and CMS displayed similar morphologies in the CPC and CPD samples, the former had higher SSAs due to their more homogeneous shapes. The aggregation of nanoparticles (approximately 150 nm) in CMS provided the highest SSA (36.7 $m^2\ g^{-1}$, Table 1). Unlike CPC, CPD was composed of two different oxide particles. On the basis of the XRD results (Fig. 1(B)), we believe that the small spherical particles with approximate diameters of 200 nm are mainly MgO whereas the blocks consist of CaO as the major component. The morphologies of MC and CaO–SBA-15 are very similar to those reported in the literature.[16,22] TEM was used to obtain more detailed insights into the structures of CPC and CPD and determine the reason for their high activities in transesterification. The TEM images (Fig. 3) indicated no porous structure in the individual particles of CPC and CPD compared with those of CaO–SBA-15 and MC.[16,22] Interestingly, CPC and CPD exhibited densely and irregularly pitted and layered structures compared with the calcined natural minerals (CC and CD). When CPC and CPD were reused and regenerated five times, conspicuous morphological changes occurred in the regenerated calcined porous calcite (RCPC) and regenerated calcined porous dolomite (RCPD). The original porous structures collapsed and were replaced by agglomerations of bulk particles (Fig. 2).

Characterization of the pores was performed by the BJH method and the detailed data are summarized in Table 1. All of the samples presented in Fig. 4 showed type III isotherms with type H_3 hysteresis loops except for MC and CaO–SBA-15 (Fig. S3†), which did not exhibit any limiting adsorption at high P/P_0 values or a plateau on the adsorption branch. This finding shows that the irregular slit-shaped pores are formed by the aggregation of plate-like particles,[23] as confirmed by the SEM and TEM results. MC and CaO–SBA-15 (Fig. 4 and Fig. S3†)

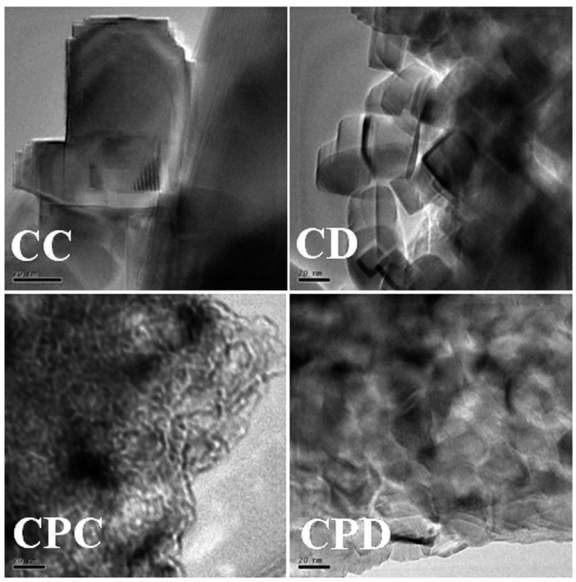

Fig. 3 TEM images of calcined calcite (CC), calcined dolomite (CD), calcined porous calcite (CPC), and calcined porous dolomite (CPD).

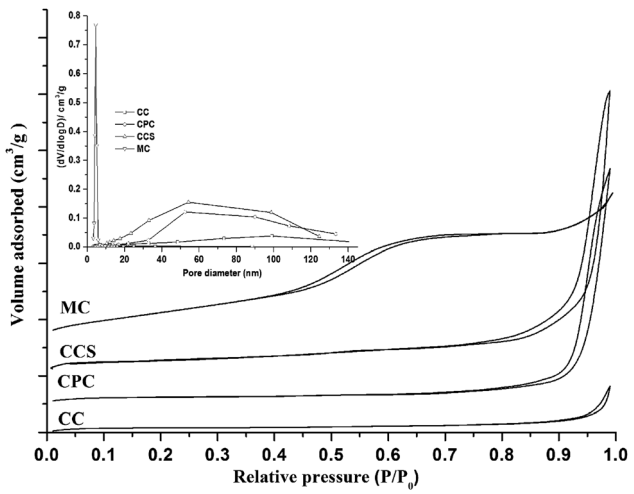

Fig. 4 N_2 adsorption–desorption isotherms and BJH pore size distributions (inset) of catalyst samples: calcined calcite (CC), calcined porous calcite (CPC), calcined calcium stearate (CCS), and mesoporous CaO (MC).

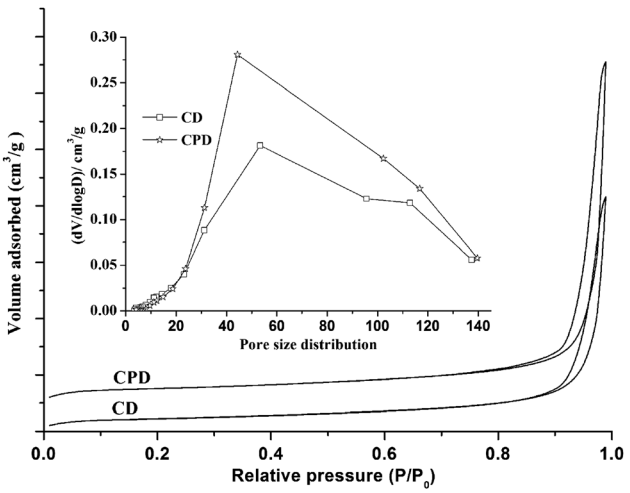

Fig. 5 N_2 adsorption–desorption isotherms and BJH pore size distributions (inset) of calcined dolomite (CD) and calcined porous dolomite (CPD).

Table 1 Physicochemical properties of the catalyst samples

Catalysts	SSA[a] ($m^2\ g^{-1}$)	AD[b] (nm)	PV[c] ($cm^3\ g^{-1}$)	Crystal size (nm)	ASD ($\mu mol\ g^{-1}$)	Hammett basicity
CC	4.1	52.8	0.02	58	66	$8.2 < pK_{BH+} < 10.1$
CD	14.3	41.3	0.06	37	42	$8.2 < pK_{BH+} < 10.1$
CCS	11.1	31.3	0.13	35	101	$8.2 < pK_{BH+} < 10.1$
CMS	36.7	23.6	0.20	23	9	$8.2 < pK_{BH+} < 10.1$
CPC	8.7	32.4	0.07	40	96	$8.2 < pK_{BH+} < 10.1$
CPD	22.1	36.7	0.13	27	71	$8.2 < pK_{BH+} < 10.1$
CaO–SBA-15	243.9	9.6	0.58	—	22	$8.2 < pK_{BH+} < 10.1$
MC	72.4	4.4	0.16	24	104	$8.2 < pK_{BH+} < 10.1$

[a] SSA: special surface area. [b] AD: average pore diameter. [c] PV: pore volume.

displayed type IV isotherms, revealing that these two materials contain uniform mesopores.[23] Fig. 4 and 5 show increased steepness and sizes of hysteresis loops when CPC and CPD were synthesized from the stearates of calcite and dolomite. The condensation steps of CPC and CPD shifted to lower relative P/P_0 values than those of the directly calcined minerals, which have smaller pores. These results were further confirmed by the pore size distribution (Fig. 4, 5 and Fig. S3†). From the pore size distribution curves, we intuitively found that all of the materials derived from natural minerals contained both mesopores and macropores. Therefore, these materials did not show SSAs as large as those of MC (72.4 $m^2\ g^{-1}$) and CaO–SBA-15 (243.9 $m^2\ g^{-1}$). Nevertheless, CPC, CPD, CCS, and CMS, had higher SSAs (Table 1) than either CC or CD because of their smaller interparticle voids and denser layers. MC and CaO–SBA-15 contained uniform mesopores in individual particles, as reported in the literature.[16,22]

CC, CPC, and RCPC were further characterized by XRD and XPS to clarify the reason for the catalyst enhancement and deactivation observed. In contrast to the XRD pattern of CC (Fig. S4†), no new species phase was observed in CPC and RCPC. The detailed surface composition information of CC, CPC, and RCPC were collected by XPS (Fig. 7). The O1s peaks located at 528.7 ± 0.1 eV and 531.3 ± 0.3 eV were assigned to the framework O^{2-} and OH^- of the CaO. The Ca peaks with binding energies close to 346.2 eV and 349.5 eV were determined to be those of $Ca(OH)_2$ species. $CaCO_3$ species was also observed.[24] The presence of CO_3^{2-} and OH^- was due to pollution that inevitably occurs during operation. Although slight changes were observed in the peak profile, no significant variation in the binding energies of the three samples was observed. Different from calcite, dolomite was mainly composed

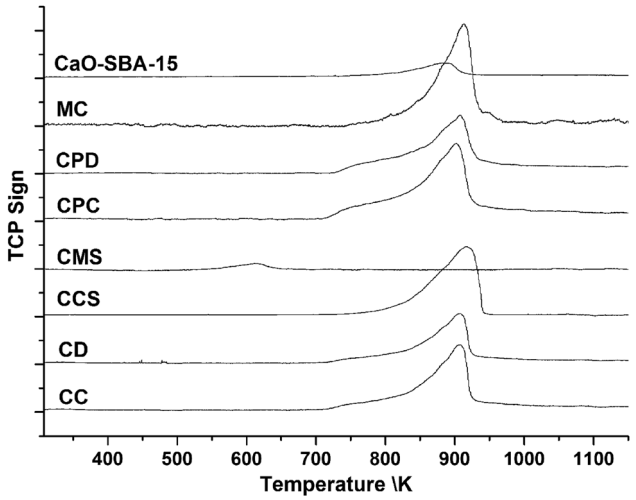

Fig. 6 CO_2-TPD curves of catalyst samples: calcined calcite (CC), calcined dolomite (CD), calcined calcium stearate (CCS), calcined magnesium stearate (CMS), calcined porous calcite (CPC), calcined porous dolomite (CPD), mesoporous CaO (MC) and CaO–SBA-15.

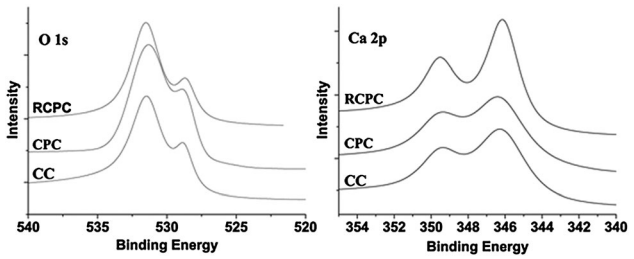

Fig. 7 O1s and Ca2p X-ray photoelectron spectra of calcined calcite (CC), calcined porous calcite (CPC), and regenerated calcined porous calcite (RCPC).

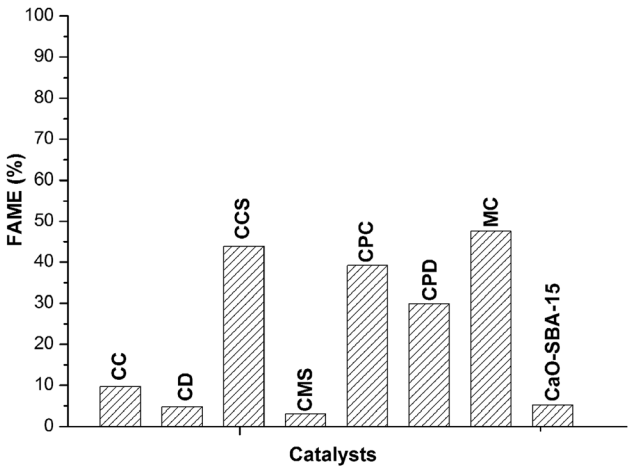

Fig. 8 JCO transesterification conversion of all catalyst samples (conditions: JCO, 50.00 g; catalyst, 0.50 g; methanol-to-oil molar ratio, 10 : 1; and 338 K for 3 h).

of calcium magnesium carbonate $CaMg(CO_3)_2$, not the major $CaCO_3$. To investigate the enhanced approach of CPD by stearic acid, the bulk and surface Mg : Ca ratio of dolomite, CD, and CPD were determined by atomic absorption and XPS. In dolomite, CD, and CPD, the bulk Ca : Mg atomic ratios were 1.16, 1.16, and 1.17, respectively. But obvious change took place in the surface Ca : Mg atomic ratios of three samples, dolomite (2.9), CD (1.21), and CPD (0.91). Compared to CD, more MgO particles were dispersed on the surfaces of CPD after modification by stearic acid. Compared to the low transesterification activities of calcined magnesium stearate (Fig. 8) and MgO,[9] we attributed increased activity of CPD to the increased special surface area of the CaO contained in the catalyst samples. On the basis of the XRD, SEM, and CO_2-TPD results (Fig. 1, 2, 6 and Fig. S4†), we can conclude that the enhanced activities of the modified catalysts and the deactivation of the reclaimed catalysts are related to the physical textures of the materials, not their chemical properties.

Catalytic activity for the transesterification reaction

All catalyst samples were rationally evaluated under the same transesterification conditions at a catalyst amount of 1 wt%, methanol-to-oil molar ratio of 10 : 1, and 338 K for 3 h. FAME content was used as the indicator. Fig. 8 shows that the modified catalysts (CPC and CPD), which featured increased SSA and ASD derived from the reaction mixtures, showed higher transesterification activities than the directly calcined minerals (CC and CD). Taking the case of CPC, the reaction conversion rate drastically increased to 39.21%, compared with the 9.75% of CC, indicating that the porous structure enhanced the catalytic performance of the accessible base sites. Although CPD possessed a higher SSA (22.1 $m^2\ g^{-1}$) than CPC, we attributed the lower FAME content (29.92%) to its lower ASD (71 $\mu mol\ g^{-1}$, Table 1), which results from inactive MgO.[25] Interestingly, MC, which features the lowest average pore diameter (4.4 nm), showed higher catalytic activity than the modified catalysts. CaO–SBA-15, which shows the highest SSA (243.9 $m^2\ g^{-1}$), provided low FAME content (5.21 wt%). These findings can be interpreted in terms of the difference between MC and mesoporous silica; CaO exhibits a strong basic character and effectiveness for transesterification reactions. Consequently, the highest transesterification activity of MC with a small pore size (4.4 nm) was due to its high external SSA (30.8 $m^2\ g^{-1}$, t-plot method). Long, isolated, parallel, and small channels in CaO–SBA-15 resulted in mass transfer limitations and counterbalancing of its high SSA (243.9 $m^2\ g^{-1}$), which is in good agreement with the literature.[15] To further reveal the relationship between catalyst structure and performance in the present study, the turnover frequencies (TOFs ($g(oil)\ h^{-1}\ g(cat)^{-1}$)) were calculated based on the mass of oil and catalyst used in the transesterification reaction. The results were as follows: CC (3.25), CD (1.59), CCS (14.63), CMS (1.01), CPC (13.07), CPD (9.96), MC (15.86), and CaO–SBA-15 (1.73). From the TOF and XPS results of CPC and CPD, we can further validate the fact that CPD, with higher SSA, showed a lower performance compared to CPC. In sum, catalyst efficiency is always closely correlated with their structural texture and active species. Only the effects of the catalyst amount and reaction time on CPC and CPD were further investigated because CCS and MC are not practical for biodiesel production.

Fig. 9 illustrates the effect of catalyst amount on transesterification in the presence of CPC, CPD, CC, and CD.

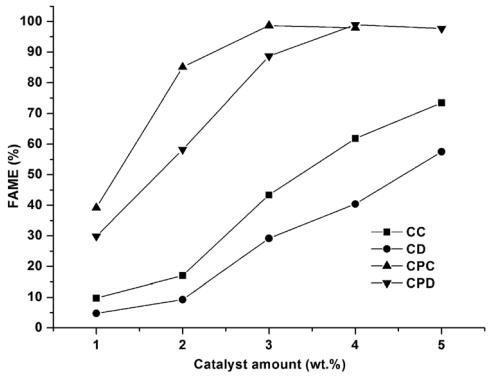

Fig. 9 Effect of catalyst amount on the conversion of calcined calcite (CC), calcined dolomite (CD), calcined porous calcite (CPC), and calcined porous dolomite (CPD) (conditions: JCO, 50.00 g; methanol-to-oil molar ratio, 10 : 1; and 338 K for 3 h).

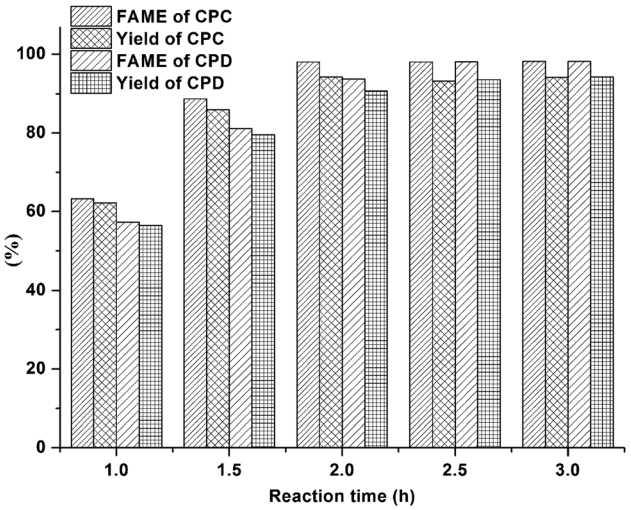

Fig. 10 Effect of reaction time on the conversion and yield of calcined porous calcite (CPC) and calcined porous dolomite (CPD) (conditions: JCO, 50.00 g; methanol-to-oil molar ratio, 10 : 1; and 338 K for 3 h).

Significant differences in catalytic performances were observed between the modified catalysts and the calcined minerals. More than 98% FAME was achieved with 3 wt% CPC and 4 wt% CPD. However, as the amounts of CPC and CPD were further increased, saponification occurred, resulting in low yields. On the other hand, less than 80% FAME was produced with 5 wt% CC and CD. This result can be supported by the CO_2-TPD data (Fig. 6 and Table 1). The relationship between FAME and reaction time is demonstrated in Fig. 10. When 3 wt% CPC was used, satisfactory FAME (98.03%) and yield (94.19%) were achieved within a relatively short time of 2 h. To achieve the same level with 4 wt% CPD, 2.5 h was sufficient time for the reaction. It indicates that the reaction rate is promoted by the accessible active sites in CPC with large ASD (96 μmol g^{-1}) and AD (36.4 nm), as proposed by Wilson *et al.*[15] In summary, the following optimized reaction conditions of CPC and CPD were determined: 3 wt% CPC or 4 wt% CPD, methanol-to-oil molar ratio of 10 : 1, and 338 K for 2 or 2.5 h. The raw oils from ELO and DSSKO were also tested on CPC and CPD under these optimized conditions, yielding 97.41% and 98.27% FAME, respectively.

The activities of the heterogeneous catalysts are weaker than those of the homogeneous species because of mass transfer limitations. Therefore, the catalytic behavior of CPC and CPD needs to be studied. Two systematic experiments were designed and performed, and the FAME content (wt%) of the products was used as an indicator of the catalytic behavior of CPC and CPD. First, filtrates of CPC, CC, CPD, and CD were prepared as follows: 1.50 g of CPC, CC, CPD, or CD was individually added to methanol (17.26 g). The mixtures were stirred (600 r min^{-1}), refluxed for 1 h under N_2 atmosphere, and then cooled in an ice-salt bath. The catalyst was quickly removed by filtration. Second, 50.00 g of JCO was added to each of the respective filtrates, and the mixtures were refluxed for 1 h in inert atmosphere (N_2). Finally, FAME contents of 6.24, 6.13, 3.94, and 4.75 wt% were obtained from CPC, CC, CPD, and CD, respectively. In the other experiment, the leaching of calcium and magnesium in biodiesel samples synthesized from 3 wt% CPC or CC for 2 h or 4 wt% CPD or CD for 2.5 h was determined and compared. Leaching results of CPC, CC, CPD, and CD showed that the total contents of Ca^{2+} and Mg^{2+} in the four biodiesel samples were 2.81 mg g^{-1} *vs.* 2.58 mg g^{-1} and 3.91 mg g^{-1} *vs.* 3.98 mg g^{-1}, respectively. Considering the data presented in these two experiments, we conclude that CPC and CPD show heterogeneous behavior for biodiesel synthesis similar to that of CC and CD, respectively.

Studies on reusability and regeneration were performed to investigate the potential application of CPC and CPD in biodiesel production. Fig. 11 shows the FAME contents of fresh CPC and CPD as well as their products regenerated through simple filtration, washing, and calcination 4 times. FAME contents gradually decreased from more than 98 wt% of CPC and CPD initially to 84.70 wt% and 87.29 wt% on the third run and to 43.51% and 40.47% in RCPC and RCPD on the fifth run, respectively. To explain the deterioration, the SSA values of RCPC at different cycles were analyzed to explain the decrease observed, and the results were 7.3, 6.9, 6.2, and 5.6 m^2 g^{-1}. As an example, the pore size and crystallite size of RCPC at the fifth run were 47.2 nm and 52 nm, respectively, and an obvious difference was observed compared to CPC (32.4 nm and 40 nm, Table 1). Combining the collapse of the porous structure observed in the SEM pattern (Fig. 2) and there being no significant binding energy variation between CPC and RCPC (Fig. 7), as well as their confirmed heterogeneous behavior, we attributed the deterioration of CPC and CPD to two reasons: (1) active site (CaO) poisoning because of CO_2 and H_2O; and (2) structural collapse resulting from mechanical stirring. Chemical contamination can be eliminated by recalcination but the activities of RCPC and RCPD are lower than those of CPC and CPD (Fig. 11). Therefore, the structural collapse of RCPC and RCPD was mainly responsible for the deterioration in activity observed compared to CPC and CPD.

To recover the performances of spent CPC and CPD, the used powders were collected and then reacted with both

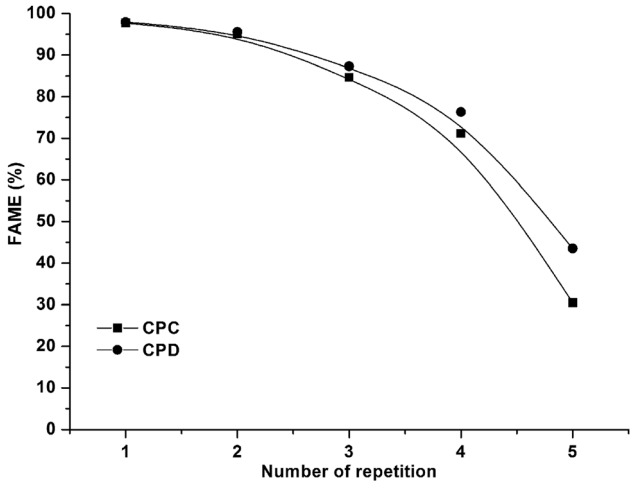

Fig. 11 Reusability of calcined porous calcite (CPC) and calcined porous dolomite (CPD) under optimized conditions (3 wt% CPC or 4 wt% CPD, methanol-to-oil molar ratio of 10 : 1; and 338 K for 2 or 2.5 h).

reclaimed and fresh stearic acid according to the catalyst preparation procedure. The powders were named stearic acid-regenerated CPC and CPD (SRCPC and SRCPD). Fig. 2 shows that SRCPC and SRCPD have shapes similar to those of fresh CPC and CPD, respectively. In addition, some important parameters of SRCPC and SRCPD were determined as follows: SSA (8.3 $m^2 g^{-1}$ and 24.7 $m^2 g^{-1}$), pore size (30.3 nm and 34.9 nm), and crystallite size (39 nm and 27 nm). The ASD value of SRCPC was 107 μmol g^{-1}. Therefore, the physicochemical properties of SRCPC were restored. The results of biodiesel synthesis using SRCPC and SRCPD were similar to those using fresh catalysts and more than 98% FAME content and 94% yield were obtained.

Conclusions

On the basis of the relationship between the catalyst efficiency and the texture structure, we developed a facile, low-cost route for the preparation of porous heterogeneous catalysts for biodiesel synthesis. CPC and CPD exhibited excellent performance by means of their high special surface areas, active site densities, and accessible active sites resulting from their porous structures. These materials offer many advantages, such as low cost, environment friendliness, and industrial applicability. We hope that the method presented here will open new perspectives for heterogeneous catalyst preparation.

Acknowledgements

This work was financially supported by the International Science & Technology Cooperation Program of China (no. 2010DFB60840), the Key Science and Technology Project of Guizhou Province (no. 20076004), and the Social Development S&T Program (no. SZ-[2009] 3011).

Notes and references

1 A. Sivasamy, K. Y. Cheah, P. Fornasiero, F. Kemausuor, S. Zinoviev and S. Miertus, *ChemSusChem*, 2009, **2**, 278–300.
2 K. Wilson and A. F. Lee, *Catal. Sci. Technol.*, 2012, **2**, 884–897.
3 P.-L. Boey, G. P. Maniam and S. A. Hamid, *Bioresour. Technol.*, 2009, **100**, 6362–6368.
4 C. Ngamcharussrivichai, P. Nunthasanti, S. Tanachai and K. Bunyakiat, *Fuel Process. Technol.*, 2010, **91**, 1409–1415.
5 K. Wilson, C. Hardacre, A. F. Lee, J. M. Montero and L. Shellard, *Green Chem.*, 2008, **10**, 654–659.
6 A. Demirbas, *Energy Convers. Manage.*, 2007, **48**, 937–941.
7 B. Yoosuk, P. Udomsap, B. Puttasawat and P. Krasae, *Bioresour. Technol.*, 2010, **101**, 3784–3786.
8 D. M. Alonso, F. Vila, R. Mariscal, M. Ojeda, M. L. Granados and J. Santamaría-González, *Catal. Today*, 2010, **158**, 114–120.
9 M. Verziu, B. Cojocaru, J. C. Hu, R. Richards, C. Ciuculescu, P. Filip and V. I. Parvulescu, *Green Chem.*, 2008, **10**, 373–381.
10 J. Montero, P. Gai, K. Wilson and A. Lee, *Green Chem.*, 2009, **11**, 265–268.
11 C. Reddy, V. Reddy, R. Oshel and J. G. Verkade, *Energy Fuels*, 2006, **20**, 1310–1314.
12 H. Sun, J. Han, Y. Ding, W. Li, J. Duan, P. Chen, H. Lou and X. Zheng, *Appl. Catal., A*, 2010, **390**, 26–34.
13 C. Samart, C. Chaiya and P. Reubroycharoen, *Energy Convers. Manage.*, 2010, **51**, 1428–1431.
14 M. Kouzu, T. Kasuno, M. Tajika, Y. Sugimoto, S. Yamanaka and J. Hidaka, *Fuel*, 2008, **87**, 2798–2806.
15 J. Dhainaut, J.-P. Dacquin, A. F. Lee and K. Wilson, *Green Chem.*, 2010, **12**, 296–303.
16 C. X. Liu, L. Zhang, J. G. Deng, Q. Mu, H. X. Dai and H. He, *J. Phys. Chem. C*, 2008, **112**, 19248–19256.
17 M. Bhagiyalakshmi, J. Y. Lee and H. T. Jang, *Int. J. Greenhouse Gas Control*, 2010, **4**, 51–56.
18 S. Takenaka, S. Sato, R. Takahashi and T. Sodesawa, *Phys. Chem. Chem. Phys.*, 2003, **5**, 4968–4973.
19 R. Wang, M. A. Hanna, W.-W. Zhou, P. S. Bhadury, Q. Chen, B.-A. Song and S. Yang, *Bioresour. Technol.*, 2011, **102**, 1194–1199.
20 M. L. Granados, M. D. Z. Poves, D. M. Alonso, R. Mariscal, F. C. Galisteo, R. Moreno-Tost, J. Santamaria and J. L. G. Fierro, *Appl. Catal., B*, 2007, **73**, 317–326.
21 Y. B. Cho, G. Seo and D. R. Chang, *Fuel Process. Technol.*, 2009, **90**, 1252–1258.
22 L. B. Sun, J. H. Kou, Y. Chun, J. Yang, F. N. Gu, Y. Wang, J. H. Zhu and Z. G. Zou, *Inorg. Chem.*, 2008, **47**, 4199–4208.
23 S. J. Gregg and K. S. W. Sing, *Adsorption, Surface Area and Porosity*, Academic press, London, UK, 2nd edn, 1982.
24 M. I. Sosulnikov and Y. A. Teterin, *J. Electron Spectrosc. Relat. Phenom.*, 1992, **59**, 111–126.
25 K. Tanabe, M. Misono, Y. Ono and H. Hattori, *New solid acids and bases: their catalytic properties*, Kodansha, Tokyo and Elsevier, Amsterdam, 1989.

Electronic Supplementary Material (ESI) for Catalysis Science & Technology

A facile, low-cost route for the preparation of calcined porous calcite and dolomite and their application as heterogeneous catalysts in biodiesel production

Rui Wang,[ab] Hu Li,[a] Fei Chang,[a] Jiafeng Luo,[a] Milford A. Hanna,[c] Daoyang Tan,[a] Deyu Hu,[a] Yuping Zhang,[a] Baoan Song,[a] and Song Yang[*a]

[a] *State-Local Joint Laboratory for Comprehensive Utilization of Biomass, State Key Laboratory Breeding Base of Green Pesticide and Agricultural Bioengineering, Center for Research and Development of Fine Chemicals, Guizhou University, Guiyang 550025, (P.R. China). Fax: (+86) 851-829-2170 E-mail: jhzx.msm@gmail.com (S. Yang)*

[b] *Food and Pharmaceutical Engineering Institute, Guiyang College, , Guiyang 550003, (P.R. China). Fax: (+86) 851-540-7613; E-mail: wangrui961@gmail.com*

[c] *Industrial Agricultural Products Center, University of Nebraska, Lincoln, NE 68583-0730, USA. Fax: 1-402-472-6338; E-mail: mhanna@unlnotes.unl.edu*

Electronic Supplementary Material (ESI) for Catalysis Science & Technology

Supporting information

Contents

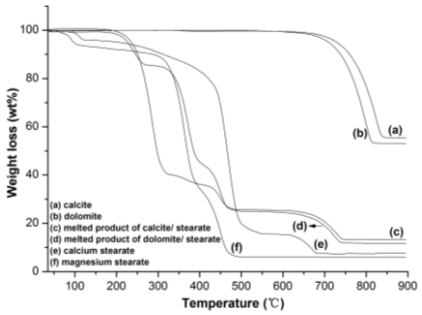

Figure S1. TGA curves of natural mines and catalyst precursors

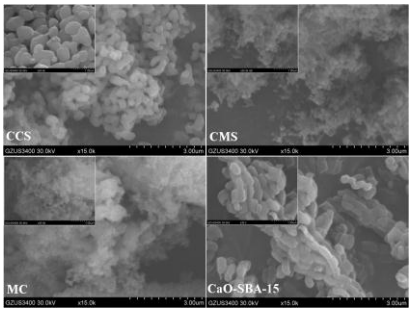

Figure S2. SEM images of calcined calcium stearate (CCS), calcined magnesium stearate (CMS), mesoporous CaO (MC), and CaO-SBA-15

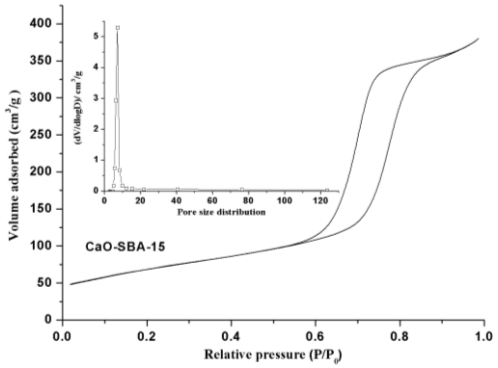

Figure S3. N_2 adsorption-desorption isotherms and BJH pore size distributions (inset) of CaO-SBA-15

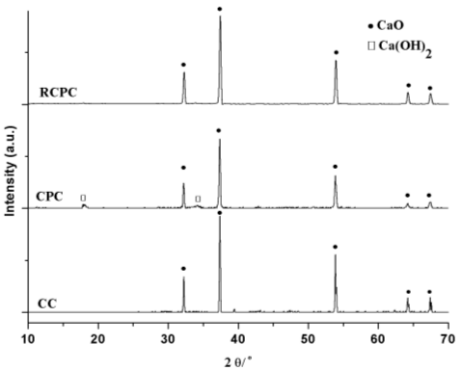

Figure S4. Wide-angle XRD patterns of catalyst samples: caclined calcite (CC), calcined porous calcite (CPC), regenerated calcined porous calcite (RCPC)